Variation of Surface Air Temperature in Complex Terrain

L. MAHRT

College of Oceanic and Atmospheric Sciences, Oregon State University, Corvallis, Oregon

(Manuscript received 11 October 2005, in final form 18 February 2006)

ABSTRACT

Data from three micronetworks with eddy correlation data and three additional micronetworks without eddy correlation data are analyzed to study the spatial variability of surface air temperature in complex terrain. A simple similarity relationship is constructed to relate the spatial variation of air temperature along the slope to the thermal forcing and mixing. Mixing is not included in present empirical formulations of the surface air temperature distribution in complex terrain. The development of surface temperature gradients along the slope, resulting from surface heating or cooling, is bounded by a maximum (or saturated) value, where a further increase of temperature gradients is restricted by redistribution of heat by thermally driven slope circulations. Although much of the spatial variation of the surface air temperature is governed by complex three-dimensionality and surface vegetation, a relatively simple relationship is able to account for much of the diurnal and day-to-day variation of the spatial distribution of air temperature. This relationship requires information on the surface heat flux and friction velocity over a reference surface. Required generalizations of the relationship are outlined before it can be applied to an arbitrary site.

1. Introduction

The spatial distribution of surface air temperature in complex terrain depends on the three-dimensional topography, vegetation, soil characteristics, net radiation, and speed of the large-scale flow. Predicting the variation of surface air temperature with surface elevation (*terrestrial temperature gradient*) is very complex, although a number of simplifications are possible for some circumstances.

Acevedo and Fitzjarrald (2001, their Fig. 3) find that a height-independent terrestrial temperature gradient is a reasonable approximation at night, subject to deviations associated with sheltering by small-scale concave curvature of the terrain corresponding to trapping of cold air in low-lying areas. Even weak curvature of the terrain can influence the local heat budget (Haiden and Whiteman 2005). Height-independent terrestrial temperature gradients have been assumed by Hocevar and Martsolf (1971), Pielke and Mehring (1977), Liston et al. (1999) and numerous other investigations. LeMone et al. (2003) find that over gentle terrain in south central Kansas, the nocturnal air temperature at 2 m is generally a linear function of surface elevation, corresponding to the height-independent terrestrial temperature gradient. Deviations from the linear dependence of air temperature on surface elevation were related to variations of vegetation and pooling of cold air in low-lying areas.

Valleys with steeper slopes are more protected from the overlying ambient flow and are less coupled to the free-atmospheric vertical temperature gradient. Acevedo and Fitzjarrald (2001) relate the nocturnal air temperature to the deviation of the surface height from a small-scale average. The effect of terrain curvature may correspond to flow of cold-air drainage over the top of the trapped colder air at the bottom of the slope (e.g., Heywood 1933; Yoshino 1975; Mahrt et al. 2001). Mahrt and Heald (1983) found that the nocturnal surface radiation temperature was more closely related to terrain curvature than surface elevation over undulating terrain. They also found that the role of slope angle was significant; apparently warmer air temperatures over steeper slopes result from stronger drainage flows and greater downward mixing of heat toward the surface. With significant ambient flow, they also found a downwind phase shift of the surface temperature with respect to the undulating terrain.

Slopes with larger vertical extent may be character-

Corresponding author address: Larry Mahrt, College of Oceanic and Atmospheric Sciences, Oregon State University, Corvallis, OR 97331-5503.
E-mail: mahrt@coas.oregonstate.edu

ized by a thermal belt where the surface air temperature reaches a maximum, often a few hundred meters above the valley floor (Yoshino 1975). Above the thermal belt, the surface air temperature decreases with surface height and may be influenced by the vertical temperature gradient of the free atmosphere. Additional discussion is provided by Whiteman (2000, see his schematic Fig. 11.4.). The thermal belt is sometimes found over the steepest part of the slope (Yoshino 1984) and is apparently caused by acceleration of cold air down the slopes, leading to shear-generated mixing of heat downward toward the sloped surface. The moderated cold-air drainage then flows out over the "cold-air lake" at the bottom of the slope. Terms, such as cold-air lake and thermal belt, are not precisely defined. In fact, Whiteman (2000) points out that nocturnal surfaces of constant potential temperature in valleys bend upward toward the side slopes in contrast to the water analogy. Greater cooling of the air at the bottom of valleys with convex side slopes, as compared with those with concave side slopes, can be produced by the smaller volume of air in the valleys with convex sidewalls, as noted by Whiteman (2000).

Values of the nocturnal terrestrial temperature gradient vary dramatically. For three selected nights, Acevedo and Fitzjarrald (2001, their Fig. 5) found that the terrestrial potential temperature gradient was about 10 K $(100\ \text{m})^{-1}$ over a surface elevation range of 50 m. Richardson et al. (2004) find that along the slopes of the largest topographical features in the northeastern United States, extending 1500 m vertically, the nocturnal terrestrial potential temperature gradient is only about 0.5 K $(100\ \text{m})^{-1}$. They averaged over all of the nights, including cloudy, windy nights. Clements et al. (2003) found a very large value of 32 K $(100\ \text{m})^{-1}$ in a 150-m-deep sinkhole. Yoshino (1984) reported that terrestrial potential temperature gradients average about 8 K $(100\ \text{m})^{-1}$ near the bottom of a slope of 700-m vertical extent with wintertime clear-sky conditions. The values were somewhat smaller in summer. For selected days over rolling landscape, examined by LeMone et al. (2003), the average value of the terrestrial potential temperature gradient was about 8 K $(100\ \text{m})^{-1}$.

The spatial variation of surface air temperature can occur simultaneously over a continuum of horizontal scales. These scales can be arbitrarily organized into smaller microscale variations such as hills, valleys, gullies and frost pockets, and larger-scale terrain forms (e.g., Kimura and Kuwagata 1993; Kurita et al. 1990). Local circulations are expected to be more dominant close to the surface and regional circulations more dominant at higher levels, if they exist (Mahrt et al. 2001). On the other hand, Whiteman et al. (2000b) found that the regional circulation associated with contrasts between the Mexican Plateau/basin and the marine air prevented normal development of local slope circulations and of strong nocturnal surface inversions. Other examples of dominance by regional circulations were found by Stewart et al. (2002). Tabony (1985) divided the impact of terrain on nocturnal air temperatures into two horizontal scales—one on the order of 3 km and less, and one on the order of 10 km. In terms of numerical models, the terrain-induced variations are partitioned into subgrid and grid-resolved variations.

The daytime spatial distribution of surface air temperature can be more complex because it is forced by solar irradiance, which depends directly on the three-dimensionality of the topography with respect to solar zenith and azimuthal angles. The effect of slope magnitude on nocturnal net radiative cooling appears to be small for weak-to-moderate slope but is significant for daytime conditions (Nie et al. 1992). In addition, spatial variations of vegetation and soil moisture can lead to dramatic variations of the daytime surface energy budget and heating of the atmosphere (Whiteman et al. 1989).

Moore et al. (1993), Thorton et al. (1997), Daly et al. (2002), and Bellasio et al. (2005) employ a specified lapse rate with a correction term for slope aspect, surface heating, and vegetation. Using a similar approach, Chung and Yun (2004) inferred that the variation of evapotranspiration contributes significantly to the variation of the relationship between air temperature and solar radiation at their sites. Bellasio et al. (2005) have incorporated the influence of surface elevation, slope aspect, and vegetation on local air temperature variations into a diagnostic meteorological model ("CALMET") and found improved comparisons with observations.

These models of the daytime spatial distribution of surface air temperature use fairly complete treatments of the solar radiation intercepted by an arbitrary inclined surface, but do not explicitly include the limiting influence of turbulent mixing and local (unresolved) transport of heat. Part of the redistribution of heat is due to local slope circulations and part is related to the influence of the larger-scale flow on mixing, such as represented by the Froude number (LeMone et al. 2003). At a given site, the terrestrial temperature gradient decreases with wind speed (Gustavsson et al. 1998), probably reflecting the influence of increased turbulent mixing. Bootsma (1976) found that, among a list of possible influences, the spatial variation of nocturnal surface temperatures was most related to wind speed and the opacity of the atmosphere.

The goal of the current study is to understand and

formulate the day-to-day variations of the terrestrial temperature gradient, as forced by surface heating/cooling and reduced by mechanical mixing and transport of heat by the regional and large-scale flow. This study will attempt to formulate such influences on the temperature distribution along the slope for possible inclusion in a model that also includes the spatial distribution of vegetation and absorption of solar radiation.

2. Data

a. Instrumentation

We analyze data from six micronetworks, which include the Hobo Pro datalogger (Onset Computer Corporation, model H08-031-08) and thermistor (Whiteman et al. 2000a; Nakamura and Mahrt 2005) enclosed in naturally ventilated multiplate shields (Davis Instruments, model 7714). Temperature measurements are taken at 0.5 m above the estimated "displacement height," taken to be a fraction of the vegetation height. The fraction was specified to decrease with increasing sparseness of the vegetation. However, because the Monin–Obukhov similarity theory is not expected to be valid above the understory, there is no theoretically based method for estimating such displacement heights and the problem remains unsolved (Nakamura and Mahrt 2005). Five-minute averages of temperature are recorded and then averaged over 1 h for the analyses of this study.

Four of the micronetworks include a limited number of Handar two-dimensional sonic anemometers that are capable of measuring wind speeds down to a few centimeters per second. Three of the micronetworks include a central tower with profiles of wind and temperature and eddy correlation measurements at one or more levels using Campbell Scientific, Inc., CSAT sonic anemometers.

b. Sites

Basic topographical information for the measurement sites is included in Table 1. The north-facing Eyerly slope in central Oregon has an average slope of about 20% (Fig. 1) over a total elevation gain of 200 m, with maximum slope occurring over the upper half of the slope. The opposing south-facing slope has an elevation gain of only about 50 m. The valley and slopes are covered by sparse ponderosa pine, part of which has been recently burned. A 17-m tower in the valley provides eddy correlation measurements at 10 m, wind profiles from Handar sonic anemometers, Hobo temperature profiles, and radiation measurements. Thirteen additional thermistors were deployed on the ground, nine of them are in a cross-valley transect. The data period extends from 6 June 2004 until 27 December 2004.

TABLE 1. Eddy correlation datasets. Averaged slope, total elevation gain, azimuth (0° is north facing), and average down-valley slope.

Site	Slope (%)	Elev gain (m)	Azimuth (°)	Down-valley slope (%)
Eyerly	20	200	0	4
Juniper	8.5	14	135	<1
Young pine	9	58	240	4
Hampton Gulley	6	11	70	1.2
Lower Starker-Bear	50	55	300	1
Upper Starker-Bear	27	800	180	1
Walnut Hill	20	90	180	0

The young pine site in central Oregon (Fig. 1) includes a transect of five Hobos extending from a gully bottom eastward up the slope, which gradually decreases with height. At higher levels, the slope becomes steeper again in association with an isolated round mountain, which was not instrumented. The height of the ponderosa pine averages about 3 m with variable density along the transect. Wind and temperature profiles, radiation, and eddy correlation data were collected from a tower on a small ridge, about 200 m to the south of the gully (Schwarz et al. 2004). The data period is from 1 April 2002 until 30 September 2002.

The juniper site in central Oregon (Fig. 1) includes a transect of four thermistors from a hilltop downward to

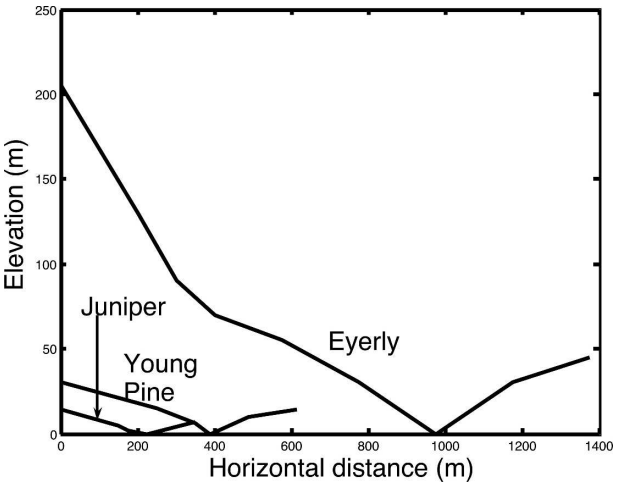

FIG. 1. Surface elevation profile for the three sites with eddy correlation data. In all three cases, the main instrumentation transect is on the left slope and extends to the top of the slope for the Eyerly and juniper sites and the top of the well-defined slope for the pine site.

the bottom of a gully, descending a vertical distance of only 14 m. The height of the sparse juniper averages about 3 m with a leaf area index (LAI) of about 1. The top of the hill had eddy correlation measurements as well as radiation data. The data period covers from 19 July 2002 to 3 November 2003.

We also collected data on three micronetworks with no eddy correlation measurements. The Walnut Hill transect is on a grass-covered south-facing slope with an average slope magnitude of 20% and a 90-m elevation gain. This site can be viewed as a miniature version of the plains–slope configuration. Fourteen Hobo thermistors were deployed along the slope in 2003. The Starker-Bear Trail dataset in the coastal range of western Oregon consists of a network within a recently planted clear cut at the bottom of a deep valley, approximately 100 m above sea level. A second transect on one of the higher slopes extends from approximately 400 to 1000 m above sea level. For this study, we have used summer data from 2002 when the network was the most complete. Fluxes over snow-covered surfaces (FLOSS) in North Park Colorado (Mahrt and Vickers 2005) included a micronetwork of eight Hobos deployed across Hampton gully, located 5 km to the north-northeast of the main tower. Eddy correlation data were collected only in winter. Here we analyze data only for the summer period.

The large-scale flow was evaluated above the local circulations at the Eyerly and pine sites, using winds measured at the top of a 31-m tower on a nearby elevated flat area. However, even at this level, the wind speed and direction varied diurnally and were significantly correlated with the slope flows at the Eyerly site. These higher-level winds seem to be part of a regional circulation responding to larger-scale slopes. A regional-scale circulation is found east of the Cascades Mountains in Washington State (Doran and Horst 1983; Doran and Zhong 1994), thought to be a combination of cold-air drainage and a larger-scale regional pressure gradient that is thermally forced by cooler air west of the Cascades. Because the diurnal variation of these regional winds and the local valley and slope flows are correlated, they do not provide statistically independent information for study of the terrestrial temperature gradient.

c. Analysis

The Hobo data were not corrected for radiatively induced temperature errors (Nakamura and Mahrt 2005) because we were unable to estimate the solar radiation for each individual thermistor in the subcanopy. For open micronetworks with no overstory, the radiatively induced errors are similar for all thermistors and are not expected to affect the estimate of the terrestrial temperature gradient. One exception is the pine site where the exposure ranges from no overstory at the bottom of the slope to sparse overstory at the top of the slope. Based on the error analysis of Nakamura and Mahrt (2005), the daytime positive radiative errors for weak winds are expected to vary from about a half degree at the bottom of the slope to a few tenths of a degree under the sparse overstory. The errors for this sensor are expected to be much smaller at night (Nakamura and Mahrt 2005). The impact of such errors are noted in section 4a.

The eddy correlation data were quality controlled using a modified version of the approach by Vickers and Mahrt (1997). The sonic anemometer data were tilt corrected using the entire dataset to compute a directionally dependent rotation angle. The fluxes were computed using a variable-averaging width described by Vickers and Mahrt (2006). Flow through the tower is allowed at the Eyerly site in order to include down- and up-valley circulations as well as up- and downslope flows. The flow through the tower occurred primarily in daytime convective conditions and did not lead to obvious contamination of the fluxes. There were no conditions imposed on the fluxes so that records were retained even with extremely small fluxes, large random flux errors, and nonstationarity.

3. Slope scaling variables

We formulate the total terrestrial potential temperature gradient as

$$\frac{\partial \bar{\theta}}{\partial z_{\mathrm{sfc}}} = \frac{\partial \Theta^*}{\partial z_{\mathrm{sfc}}} + \frac{\partial [\theta]}{\partial z}, \tag{1}$$

where $\bar{\theta}$ is the total observed potential temperature at the surface, Θ^* is the deviation of the surface potential temperature from the basic-state potential temperature $[\theta]$, and z_{sfc} is the elevation of the ground surface. The basic-state potential temperature is considered to be a function of only z while Θ^* includes the diurnal variation.

In some studies, the background ambient or basic-state stratification $\partial[\theta]/\partial z$ includes the formation of the surface inversion layer in the valley. The stratification below the maximum height of the topography is ambiguous in our datasets because of the strong height dependence and horizontal variability. Consequently, we will define the basic-state stratification to be that above the maximum terrain height. The terrestrial tem-

perature variations in our data are generally much larger than those typical of the ambient stratification, based on supplementary sounding and aircraft data for some of our field programs. As a result, determination of the basic-state stratification is of little consequence for our analysis. In contrast, LeMone et al. (2003) found it necessary to retain the background stratification in nocturnal flow over undulating terrain of the Great Plains of the United States.

A scaling variable for the variation of the surface potential temperature is posed in terms of the surface heat flux, which generates the diurnal variation of the terrestrial temperature gradient. This generation of surface air temperature differences along the slope is constrained by vertical turbulent mixing of heat away from the surface and horizontal transport of heat by the large-scale flow and the local thermally driven flow. Turbulent mixing can be posed in terms of the surface friction velocity. The surface friction velocity and the mean wind speed are highly correlated; their ratio depends on stability. The influence of the mean wind and the turbulent mixing on the variation of surface temperature are difficult to isolate. The surface friction velocity is preferable to the wind speed as a scaling velocity because it varies much more slowly with height above the ground surface than the wind speed. We therefore define the temperature scale for the terrestrial temperature variation as

$$\theta_* \equiv \frac{\overline{w'\theta'}}{u_*}. \tag{2}$$

This temperature scale is often used to scale turbulent temperature fluctuations, but here represents the above physics influencing the terrestrial temperature gradient.

The height dependence of the air temperature is most simply expressed as the difference between two surface elevations. The *terrestrial potential temperature difference* between two surface elevations can be formulated as

$$\overline{\theta}(z_{\rm sfc}) - \overline{\theta}(z_{\rm ref}) = f_1(\theta_*) f_2(z'_{\rm sfc}/D) + \frac{\partial[\theta]}{\partial z} z'_{\rm sfc}, \tag{3}$$

where

$$z'_{\rm sfc} = z_{\rm sfc} - z_{\rm ref}, \tag{4}$$

where $z_{\rm ref}$ is a reference surface elevation such as the bottom of the slope, f_1 is a function determining the magnitude of the terrestrial potential temperature gradient at the bottom of the slope, f_2 is a function determining the height dependence of the terrestrial temperature gradient, and D is a scaling depth describing this vertical variation. The function f_2 will represent the usual decrease of the terrestrial temperature gradient with increasing surface elevation. The functions f_1 and f_2 will be determined from the data.

Although Eq. (3) is useful for studying the temperature difference between stations at different surface elevations, formulations for models are more conveniently expressed in terms of the terrestrial potential temperature gradient, which becomes

$$\frac{\partial \overline{\theta}}{\partial z_{\rm sfc}} = f_1(\theta_*) f'_2(z'_{\rm sfc}/D) + \frac{\partial[\theta]}{\partial z}, \tag{5}$$

where f'_2 is the vertical derivative of f_2 with respect to surface elevation.

The above scaling requires eddy correlation measurements, which are generally not available with temperature networks. An external estimation of the forcing of the terrestrial temperature gradient, without need for eddy-correlation measurements, can be expressed in terms of the net radiation as

$$\mathrm{RF} \equiv \frac{R_{\rm net}}{\Theta_o \rho c_P V}, \tag{6}$$

where $R_{\rm net}$ is the net radiation, Θ_o is a basic-state potential temperature, ρ is the mean density, c_P is the specific heat capacity, and V is the wind speed. Here $R_{\rm net}$ could be generalized to include the influence of the slope on the net radiation perpendicular to the sloped ground surface. Application of Eq. (6) to the distribution of air temperature assumes that the spatial variation of heating/cooling of the air is proportional to the net radiation, which assumes that the differential surface heating is not influenced by the surface moisture flux. Because the heat flux more directly influences the air temperature than the net radiation, the approach based on net radiation is found to be less general than that based on θ_*.

4. Observed forcing of the terrestrial temperature gradient

We focus on the data from the Eyerly site, which is the most complete dataset, and then contrast these with the other sites. The daytime flow is normally up the valley and up the side slopes, while nocturnal flows are normally down the valley side slopes and down the valley. The nocturnal terrestrial temperature gradient at the Eyerly site is approximately constant in the lowest 100 m of surface elevation, about the lower half of the slope (section 6), and then decreases at higher elevations. Therefore, we will examine the terrestrial poten-

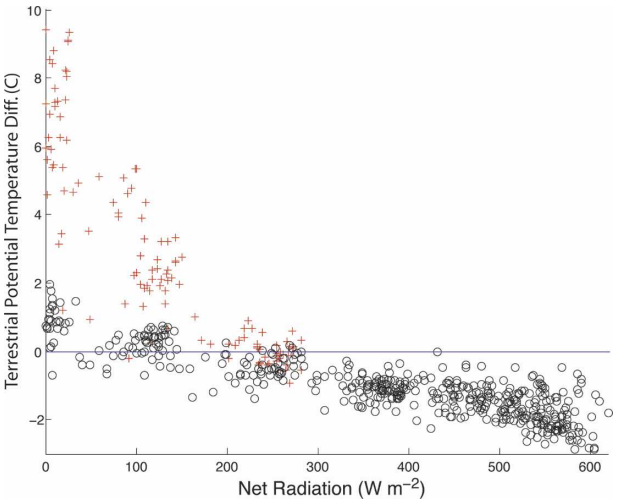

FIG. 2. Hourly values of the daytime terrestrial potential temperature difference (K) for the Eyerly site in summer as a function of the net radiation. The normally clear skies and the discretization of net radiation into hourly averages leads to clumping of the net radiation. Large positive values of the terrestrial temperature difference correspond to lingering stability during the early morning transition (red +, 0500–0800 LST). A value of −1.1 K corresponds to well-mixed conditions (adiabatic lapse rate).

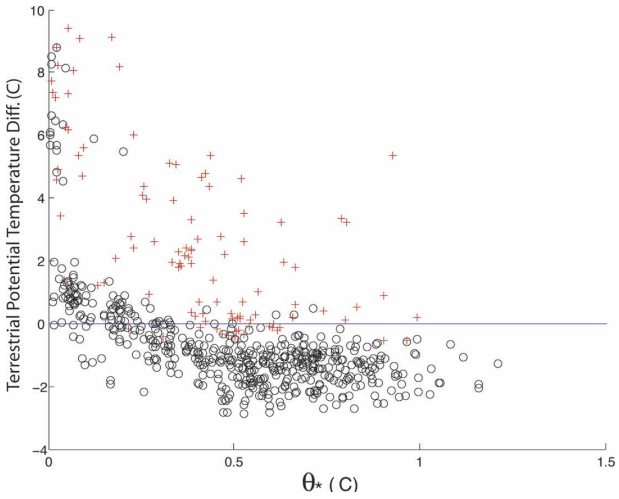

FIG. 3. Hourly values of the daytime terrestrial potential temperature difference for the Eyerly site in summer as a function of the thermal forcing θ_* [Eq. (2)]. Red pluses identify observations during the morning transition period (0500–0800 LST). A value of −1.1 K corresponds to well-mixed conditions.

tial temperature difference [Eq. (3)] between the temperature station at approximately 110 m above the bottom of the slope and the temperature at the bottom of the slope. In contrast to nocturnal conditions, the daytime terrestrial temperature gradient is approximately independent of surface elevation for most of the slope, not just the lowest 100 m.

For the short slope at the juniper site, the terrestrial temperature gradient decreases slightly with increasing surface elevation. For this short slope, we represent the terrestrial temperature gradient in terms of the thermistors at the top and the bottom of the slope. The terrestrial temperature gradient at the pine site generally decreases with surface elevation. We examine the potential temperature difference between the top and the bottom of the slope at the pine site. At the juniper and pine sites, the slope circulations were less dominant than at the Eyerly site, possibly because of shorter slopes (Table 1).

a. Daytime heating

Because the Eyerly site is dry in summer, the surface heat flux increases systematically with increasing net radiation with only modest scatter. As a result of the strong interrelationships between variables at this site, the daytime terrestrial temperature difference is highly correlated to the net radiation (Fig. 2). Inclusion of information on the wind or friction velocity does not improve the prediction of the terrestrial temperature difference for summer daytime conditions at this site. However, the close relationship between the daytime terrestrial temperature difference and the net radiation neither extends to other seasons nor to other sites, particularly when the surface latent heat flux reduces the surface heating. For these other sites and seasons, the daytime terrestrial temperature difference is more closely related to the thermal forcing θ_* than net radiation.

For the Eyerly site, the daytime negative terrestrial temperature difference increases approximately linearly with increasing thermal forcing θ_* [Eq. (2)] until the terrestrial potential temperature difference reaches a "saturation" value of about −1.5 K at a value of the thermal forcing of about 0.7 K (Fig. 3). The terrestrial temperature gradient becomes independent of further increases of the thermal forcing, though with substantial scatter. Apparently with sufficient heating, the terrestrial temperature gradient becomes limited by convective mixing and redistribution of heat by the upvalley and upslope circulations. We can therefore define a *maximum or saturation value of the terrestrial temperature gradient.* For cases in the saturation regime, the friction velocity tends to be proportional to the surface heat flux.

The large, positive values of the terrestrial temperature gradient at the Eyerly site (red pluses, Fig. 3) are associated with the early morning transition when the heat flux has become positive at the bottom of the slope but the stratification along the north slope is still stable.

TABLE 2. Saturation or maximum values of the thermal forcing $[(\theta_*)_U, (\theta_*)_S]$ [K (100 m)$^{-1}$] and the corresponding saturation or maximum values of the terrestrial potential temperature gradients $[(\partial\Theta^*/\partial z_{\rm sfc})_U, (\partial\Theta^*/\partial z_{\rm sfc})_S$; K (100 m)$^{-1}$], where U and S refer to unstable and stable conditions. The scaling depth D is defined in Eq. (8) and was estimated visually by plotting the analytical function for different values of D. For comparison with other studies, the terrestrial potential temperature gradients are reported [K (100 m)$^{-1}$], even though the total vertical extent of the slope at the pine and juniper sites is much less than 100 m (Table 1). The relationships for the summer and winter Eyerly site are indistinguishable.

Site	$(\theta_*)_U$	$(\partial\Theta^*/\partial z_{\rm sfc})_U$	$(\theta_*)_S$	$(\partial\Theta^*/\partial z_{\rm sfc})_S$	D
Eyrely summer	0.7	−1.8	−0.15	+10	110
Eyrely winter	0.7	−1.8	−0.15	+10	110
Juniper summer	0.3	+2.2	−0.15	+25	14
Juniper winter	0.3	+2.0	−0.1	+23	14
Pine	0.3	+1.5	−0.2	+12	30

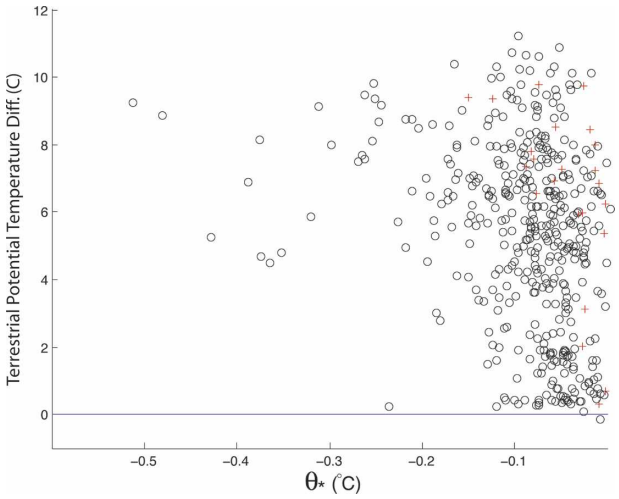

FIG. 4. The nocturnal terrestrial potential temperature difference for the Eyerly site in summer as a function of the thermal forcing [Eq. (2)]. Red pluses identify observations during the morning transition period (0500–0800 LST) where the terrestrial potential temperature difference is still positive (stable). A value of −1.1 K corresponds to well-mixed conditions (adiabatic lapse rate).

For winter conditions at this site, the terrestrial temperature gradient does not reach saturation conditions, but within the range of winter values of θ_* follows the same dependence on θ_* as in summer.

In contrast to the Eyerly site, the daytime surface potential temperature at the juniper and pine sites increase with surface elevation. Air temperatures at the pine site are warmer in areas with a sparse pine overstory as compared with absence of overstory at the bottom of the slope, corresponding to an increase of potential temperature with increasing surface elevation. Apparently the overstory is sufficiently sparse to allow for significant heating of the surface, but reduces ventilation of the near surface air to allow more heat buildup at the surface relative to open areas. The increase of temperature up the slope at the pine site could be underestimated by a few tenths of a degree because of the increase of overstory and decrease of radiatively induced thermistor errors up the slope (section 2c). The positive values of the daytime terrestrial potential temperature gradient at the pine and juniper sites increase with thermal forcing up to a saturation value and then become independent of the thermal forcing for larger values. However, the relationship of the terrestrial temperature gradient to the thermal forcing at the juniper and pine sites is characterized by more scatter in comparison with the larger slope at the Eyerly site. Nonetheless, saturation values were definable at the juniper and pine sites (Table 2, section 8).

b. Nocturnal temperature distribution

The nocturnal terrestrial temperature difference at the Eyerly site is poorly related to the narrow range of values of net radiation and is less related to the thermal forcing in comparison with daytime conditions (Fig. 3) and requires bin averaging of the data to reveal the dependence of the terrestrial temperature difference on the thermal forcing (not shown). The scatterplot does reveal that the terrestrial temperature difference is bounded from below by a minimum value, which increases systematically with increasing magnitude of the thermal forcing θ_*, as seen from the envelop of points in Fig. 4. The overall relationship is weak because of numerous large values of the terrestrial temperature difference occurring with weak thermal forcing. The generally poor relationship for nocturnal conditions may be due to the dominance of the total mean flow by the drainage circulations. As a result, the total wind speed and u_* are both closely related to the downward heat flux, in which case θ_* is no longer a useful discriminator. For the juniper site, where drainage circulations are less evident and the mean flow is more dominated by the larger-scale wind, the nocturnal terrestrial temperature gradient is more closely related to θ_* (Fig. 5), although the scatter remains large. Large random flux errors for the weak nocturnal fluxes also contribute to the scatter in the relationship between the terrestrial temperature gradient and θ_*.

The nocturnal terrestrial temperature difference is also related to the thermal forcing for the winter juniper data and the summer pine data (winter data are not available at the pine site), although the terrestrial temperature difference increases with the magnitude of the thermal forcing for the entire range of the thermal forc-

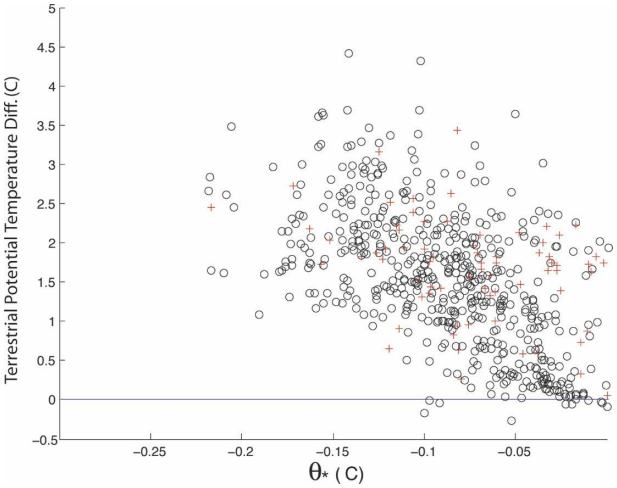

FIG. 5. The nocturnal terrestrial potential temperature difference for the juniper site in summer as a function of the thermal forcing [Eq. (2)]. A value of −0.14 K corresponds to well-mixed conditions (adiabatic lapse rate).

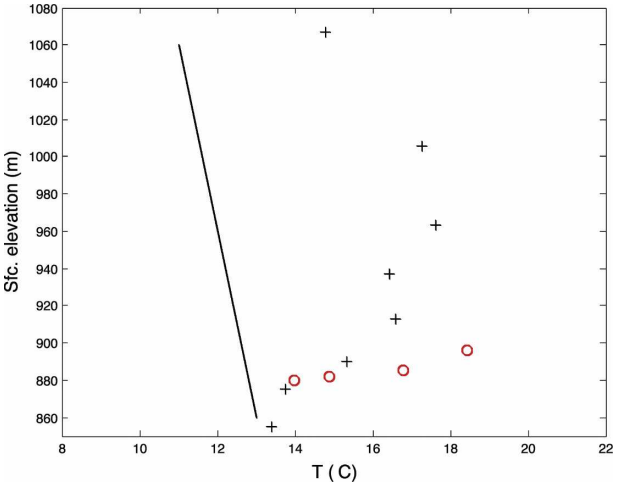

FIG. 6. Composited height distribution of the temperature for the Eyerly site for late-evening conditions (0000–0400 LST) for a 38-day period when the higher two temperature stations were operating. The red circles are the temperatures on the tower. The solid line is an adiabatic temperature profile corresponding to well-mixed conditions. The terrestrial temperature gradient statistics reported in Table 2 are computed for the 960-m level and below where a longer dataset is available and the terrestrial temperature gradient is more constant.

ing for both of these datasets. Because there is no range of thermal forcing where the terrestrial temperature gradient becomes independent of the thermal forcing for the pine and winter juniper sites, the nocturnal maximum values of the terrestrial potential temperature gradient are reported in Table 2 in place of the saturation values in section 8.

A much smaller magnitude of the thermal forcing at night generates a much larger magnitude of the terrestrial temperature gradient relative to daytime values. Weak downward nocturnal heat fluxes create greater along-slope variations of air temperature in comparison with the large heat fluxes in the daytime when both horizontal and vertical mixing is greater.

The nocturnal terrestrial temperature gradient varies only slowly with height for the lower half of the slope at the Eyerly site (Fig. 6). The larger vertical gradient of temperature on the tower above the valley floor relative to the terrestrial temperature gradient corresponds to lower temperatures in the downslope flow relative to the temperatures at the same level above the valley (Fig. 6). Whiteman (2000) and others have also found that the nocturnal terrestrial temperature gradient on small scales can be much smaller than the vertical temperature gradient away from the slope such that surfaces of constant potential temperature tended to be horizontal over the valley and more parallel to the slope surface at the valley sidewalls. Similarly, the daytime unstable stratification above the valley floor is much larger than the negative terrestrial temperature gradient at the Eyerly site (Fig. 7) so that the upslope flow is warmer than the temperature at the same height above the valley floor.

5. Formulation of the dependence on the thermal forcing

Based on the concept of a saturation terrestrial temperature gradient, we formulate the terrestrial potential temperature gradient [Eq. (1)] to be a linear function of the thermal forcing up to the saturation value and con-

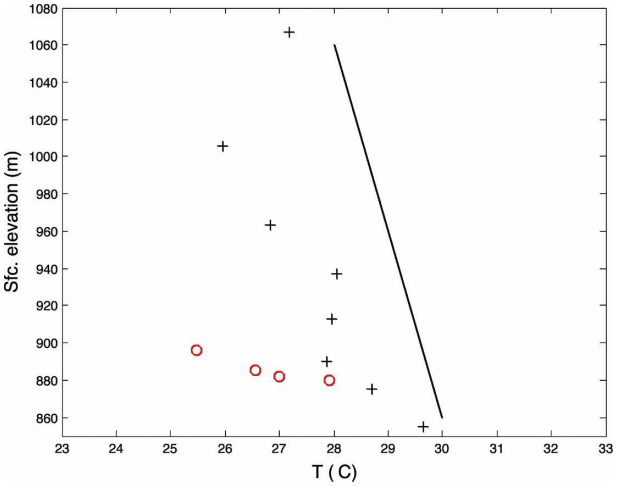

FIG. 7. Composited height distribution of the temperature for midday (1100–1600 LST) at the Eyerly site. The red circles are the temperatures on the tower. The solid line is an adiabatic temperature profile. See Fig. 6 for additional explanation.

stant for larger values. With this approach, $f_1(\theta_*)$ in Eq. (5) is formulated as

$$\left(\frac{\partial\Theta^*}{\partial z_{\rm sfc}}\right)_U \frac{\theta_*}{(\theta_*)_U}; \quad 0 < \theta_* < (\theta_*)_U$$
$$\left(\frac{\partial\Theta^*}{\partial z_{\rm sfc}}\right)_S \frac{\theta_*}{(\theta_*)_S}; \quad (\theta_*)_S < \theta_* < 0, \tag{7}$$

where the subscript U refers to the saturation or maximum value of the thermal forcing for daytime unstable conditions and the corresponding terrestrial potential temperature gradient at the bottom of the slope ($z'_{\rm sfc} \rightarrow 0$). The subscript S refers to the values for nocturnal stable conditions. For magnitudes of the thermal forcing (θ_*) greater than the saturation value, the terrestrial temperature gradient is approximated as the saturation value, independent of the forcing value.

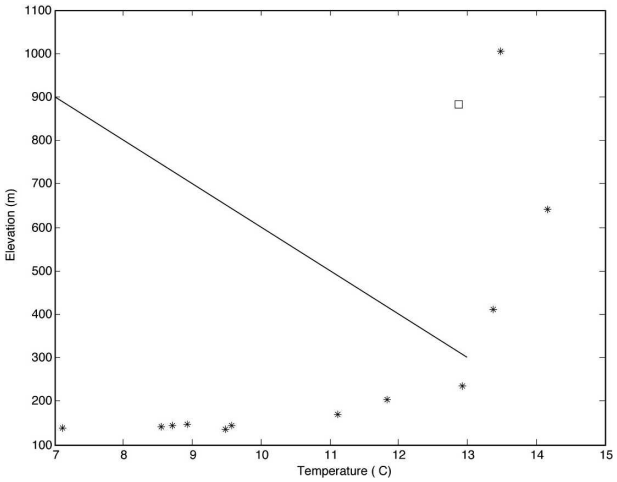

FIG. 8. The averaged height distribution of surface air temperature for the Starker-Bear micronetwork for summer at midnight. The black line is an adiabatic temperature profile. The square indicates a station on the north-facing slope.

6. Height dependence of the terrestrial temperature gradient

At the Eyerly site, the nocturnal terrestrial temperature gradient at midslope decreases with height and reverses sign corresponding to a thermal belt where the temperature reaches a maximum with respect to surface elevation (Fig. 6). For a greater variety of topographical situations, we include data from the sites without eddy correlation data. The Walnut Hill site and the Starker-Bear transect both include frequent data with marine air penetration. To crudely filter out cloudy and windy days, which were not common in the other datasets, we use only days when the diurnal variation exceeds the average diurnal variation. On the Walnut Hill slope, the nocturnal terrestrial temperature gradient decreases with height to very small values at midslope but does not reverse sign. Well-defined drainage flow is also common on this slope. The terrestrial temperature gradient decreases more gradually with surface elevation when compared with the slopes at the pine, juniper, and Hampton Gulley sites. The total vertical extent of these slopes is below the relative height of the thermal belt at the Eyerly site.

For a higher, more isolated mountain extending well above the surrounding terrain, the terrestrial temperature gradient becomes smaller and more significantly influenced by the background stratification of the free air. This is illustrated with the higher part of our site with the largest vertical elevation change (Starker-Bear transect, section 2b). The nocturnal terrestrial temperature gradient is large in the first few hundred meters above the valley floor (Fig. 8) and is much smaller above this level. This level is somewhat below the averaged ridge top. The temperature at the second highest site (square in Fig. 8) is probably cooler than the surrounding area because it is in a gully on the north side of the slope. The height dependence of the terrestrial temperature gradient is more difficult to define in the daytime, partly because it is smaller than the nocturnal values and partly because it is more sensitive to changes of vegetation and slope magnitude and aspect (section 8).

Based on the six micronetworks and the literature, the form of the height dependence of the terrestrial temperature gradient is unique to every slope and dependent on the three-dimensionality of each slope. It is not practical to define a different function, $f_2(z'_{\rm sfc}/D)$, for every slope. Even at a given slope, $f_2(z'_{\rm sfc}/D)$ appears to vary diurnally and weakly with season. Restricting the formulation of the height dependence to a single free parameter, the decrease of the terrestrial potential temperature gradient with height is crudely represented with an exponential decrease, such that

$$f'_2(z'_{\rm sfc}/D) = \exp[-(z'_{\rm sfc}/D)]. \tag{8}$$

The visual best-fit value of D, based on plotting the function with different values of D, appears to be roughly comparable to the height of the local ridge tops, although more sites are needed before such a conclusion can be made with any confidence. Based on the composited vertical structure of the temperature, the value of D is chosen to be 110 m for the Eyerly site, the height of the slope for the juniper site, and the approximate height of the highest station for the pine site (Table 2). The exponential fit is a reasonable approxi-

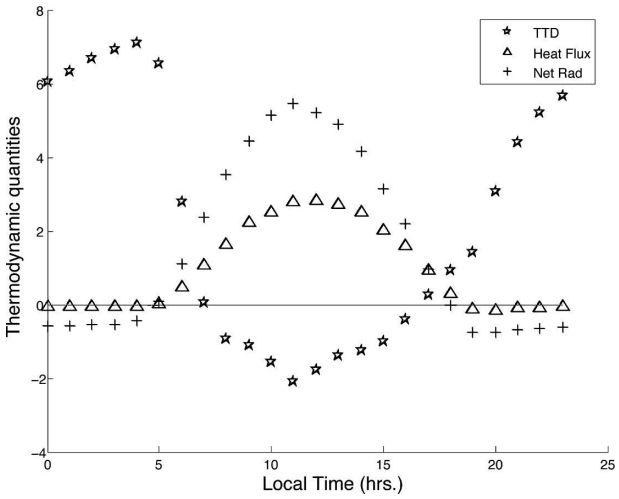

FIG. 9. Summer diurnal variation at the Eyerly site for the terrestrial potential temperature difference (K, stars), the heat flux (K m s^{-1} $\times$ 10, triangles), and the net radiation (W m^{-2}/100; pluses) for the conditionally selected days.

mation for the Walnut Hill site but is not a good fit for the pine site or Starker-Bear site, where the upper part of the slope is above the surrounding ridges. Better approximations could be obtained with more complex functions with more than one free parameter.

7. Diurnal evolution

The relationship between the terrestrial temperature difference [Eq. (3)] and the thermal forcing breaks down in the early morning transition, which represents the largest deviations from Eq. (7). For example, at the Eyerly site, the terrestrial temperature gradient lags (0700 LST) the sign reversal of the net radiation and heat flux (0500 LST) by about by about 2 h (Fig. 9). The morning transition for individual days is even sharper than indicated by the composited diurnal variation because of the variation of sunrise within the data period and because the occurrence of the transition time with respect to sunrise varies between days. The sharpness of the morning transition could be related to sufficient weakening of the surface inversion to allow sudden shear-driven instability (Lenschow et al. 1979).

The lag of the positive terrestrial temperature gradient in the morning transition at the Eyerly site can be approximated with a correction term to Eq. (7) of the form

$$\left(\frac{\partial\overline{\theta}}{\partial z_{\rm sfc}}\right)_n \exp\left(-\frac{\tau}{\tau_o}\right), \tag{9}$$

where n refers to the nocturnal value of the terrestrial temperature gradient just prior to sunrise, τ is the time after sunrise, and τ_o is the transition time scale, which is on the order of 2 h for the Eyerly site (Table 2). With winter conditions, τ_o may be much larger when elimination of the surface stratification by the weak surface heating may require longer periods. In fact, the surface stratification may not be eliminated at all during the day (Whiteman et al. 1999). Furthermore, the elimination of the nocturnal surface inversion within the valley is expected to depend on the geometry of the valley (Whiteman and McKee 1982). For the Eyerly site, the systematic error in Eq. (7) during the early evening transition is not sufficiently large to confidently model with a correction term. The early morning transition at the juniper and pine sites is more complex, indicating that Eq. (9) is not of general validity.

8. General formulation

To include the transition lag and above height dependence, Eq. (5) can be written as

$$\frac{\partial\overline{\theta}}{\partial z_{\rm sfc}} = f_1(\theta_*)\exp\left(\frac{-z'_{\rm sfc}}{D}\right) + \mathrm{LAG}\left(\frac{\tau}{\tau_o}\right) + \frac{\partial[\theta]}{\partial z}, \tag{10}$$

where f_1 is defined by Eq. (7) and the LAG term [Eq. (9)] represents the lag of the terrestrial temperature gradient behind the time-dependent heat flux during the morning transition.

As an example, we vertically integrate Eq. (10) from a reference level ($z = z_{\rm ref}$, $z'_{\rm sfc} = 0$), such as the floor of a valley. Omitting the early morning transition term and the generally much smaller basic-state stratification, integration of Eq. (10) from $z'_{\rm sfc} = 0$ to some arbitrary level z' predicts the terrestrial potential temperature difference [Eq. (3)] to be

$$\overline{\theta}(z'_{\rm sfc}) - \overline{\theta}(z_{\rm ref}) = f_1(\theta_*)D\left[1 - \exp\left(\frac{-z'_{\rm sfc}}{D}\right)\right] + \frac{\partial[\theta]}{\partial z}(z'_{\rm sfc}). \tag{11}$$

The saturated value of $f_1(\theta_*)$ is estimated by equating $f_1(\theta_*)\ D[1 - \exp(-z'_{\rm sfc}/D)]$ to the observed potential temperature difference $\overline{\theta}(z'_{\rm sfc}) - \overline{\theta}(z_{\rm ref})$ for saturated conditions. The saturated value of f_1, and therefore the saturated terrestrial temperature gradient, is then computed from values of D in Table 2. The results are recorded in Table 2.

The parameter values vary between sites by a factor of 2, which presumably reflects differences of the three-dimensional topography and vegetation between the three sites. At this point, it is not possible to model the

variation of the saturation values between sites. To further study the difference between sites, we include the noneddy correlations sites, again using only days where the diurnal temperature variation was greater than the seasonal average diurnal variation. The nocturnal terrestrial temperature gradients were largest at the bottom of the Starker-Bear transect, Hampton Gully, and juniper site, all of which area valley sites with a weak down-valley slope. The terrestrial temperature gradient was about half as large at the Eyerly site where the down-valley slope was greater and the opposing slope length is only about 15% of the north-facing slope. The nocturnal terrestrial temperature gradient is weakest at the pine site, where the opposing slope was much shorter and the down-valley slope was significant (Table 1), and at Walnut Hill, where there was no opposing slope. Magono et al. (1982) attributed extremely cold temperatures at the surface of a basin to a lack of down-valley flow.

Slope aspect and vegetation

The above prediction of the terrestrial temperature gradient for daytime conditions may require adjustment for the influence of slope aspect and vegetation. Such adjustments cannot be tied to the height dependence of the terrestrial temperature and an independent term is required, such that

$$\overline{\theta}(z) = \overline{\theta}(z)_F + G(\theta_*, M, A), \tag{12}$$

where $\overline{\theta}(z)_F$ is the value of the potential temperature predicted by Eq. (11) and $G(\theta_*, M, A)$ represents the influence of slope aspect on incident solar radiation, magnitude and curvature of the terrain, and vegetation. Here G is expected to increase with the thermal forcing θ_* because spatial variations of surface air temperature are expected to be largest with greater surface heating and less mixing and horizontal transport. The influence of spatial variations of incident solar radiation and LAI of the overstory has been included in Moore et al. (1993) and Bellasio et al. (2005).

In our datasets, the influence of the spatial variation of the incident solar radiation on the surface air temperature was definable but complicated by several additional influences. The effect of spatial variation of the incident solar radiation on the air temperature distribution is not only related to the thermal forcing but is much greater in the early morning when the mixing depth is small. At this time, the impact of differential surface heating is confined to a thin layer and has a greater impact on the air temperature distribution. In addition, south-facing slopes at our semiarid forested sites are characterized by less overstory and drier soil in comparison with the north-facing slopes. Consequently, the effects of slope aspect and vegetation are difficult to separate. Last, the impact of surface variations are greater when the horizontal scale of such variations are greater so that their impact is less vulnerable to reduction by atmospheric mixing (their blending height is higher).

9. Conclusions

The above analysis of temperature data from three different micronetworks with eddy correlation data in complex terrain indicates that the magnitude of the along-slope variation of the surface potential temperature with surface elevation (terrestrial potential temperature gradient) increases approximately linearly with increasing surface heating or cooling. The magnitude of the terrestrial temperature gradient decreases with increasing mechanical redistribution of heat resulting from vertical mixing and horizontal transport.

For a given site, the magnitude of the daytime terrestrial temperature gradient is reasonably well predicted by a thermal forcing temperature scale θ_* [Eq. (2)], defined as the ratio of the surface heat flux to the surface friction velocity. When the thermal forcing (θ_*) exceeds a saturation value, the terrestrial temperature gradient becomes independent of the forcing. Apparently, mixing and redistribution of heat by slope-generated circulations lead to a maximum or saturation value of the terrestrial temperature gradient for a given site. In the saturation regime, the flow appears to be dominated by slope circulations and u_* is proportional to the surface heat flux. However, the saturation value of the terrestrial temperature gradient varies substantially between sites and is sometimes never reached in winter. The sign of the smaller daytime terrestrial temperature gradient may be negative or positive, depending on the details of the topography and height distribution of vegetation.

For nocturnal conditions, the terrestrial temperature gradient becomes poorly related to θ_* for the Eyerly site, where the mean flow and friction velocity are dominated by the local thermally driven circulations, which in turn are proportional to the magnitude of the downward heat flux. Use of multiple velocity scales may improve the relationship for this site, although the present datasets are inadequate for construction of more complex relationships. The temperature scale θ_* is a better predictor for the other sites. The nocturnal terrestrial temperature gradient is greater on the side slopes of valleys with weaker down-valley slope, allowing buildup of cold air at the base of the slope. Exposed slopes on isolated hills have a smaller terrestrial tem-

perature gradient relative to those of the valley side slopes.

Equation (11) quantitatively represents the importance of the influence of mixing and slopes circulations on the terrestrial temperature gradient. This representation performs well at our sites in summer where the synoptic situation and diurnal cycle normally vary little between days. The generality of this approach is not known, and presumably its performance would degrade at locations with significant synoptic variability. The present approach does not work well during the early morning transition period when the surface inversion may survive well after the surface heat flux becomes positive. This approach does not include a general procedure for predicting the large variations of coefficients between different topographical situations. Toward this goal, the above formulation for the influence of mixing on the terrestrial temperature gradient needs to be combined with a model of the influences of slope orientation and vegetation on radiative forcing (section 8a). Without such a generalization, the practical use of our formulation is probably limited.

Acknowledgments. I gratefully acknowledge the very helpful comments of David Whiteman and Roberto Bellasio and greatly appreciate the useful comments of both reviewers. I also appreciate the deployment and measurement collection by John Wong at the Eyerly and pine sites and the data processing of Dean Vickers. William Tahnk and Kayge McNab assisted with the collection of temperature data on the Starker-Bear Trail. This material is based upon work supported by Contract W911NF-05-C-0067 from the Army Research Office and Grant 0107617-ATM from the Physical Meteorology Program of the National Sciences Program.

REFERENCES

Acevedo, O. C., and D. R. Fitzjarrald, 2001: The early evening surface-layer transition: Temporal and spatial variability. *J. Atmos. Sci.,* **58,** 2650–2667.

Bellasio, R., G. Maffeis, J. S. Scire, M. G. Longoni, R. Bianconi, and N. Quaranta, 2005: Algorithms to account for topographic shading effects and surface temperature dependence on terrain elevation in diagnostic meteorological models. *Bound.-Layer Meteor.,* **114,** 595–614.

Bootsma, A., 1976: Estimating minimum temperature and climatological freeze risk in hilly terrain. *Agric. For. Meteor.,* **16,** 425–443.

Chung, U., and J. I. Yun, 2004: Solar irradiance-corrected spatial interpolation of hourly temperatures in complex terrain. *Agric. For. Meteor.,* **126,** 129–140.

Clements, C. B., C. D. Whiteman, and J. D. Horel, 2003: Cold-air-pool structure and evolution in a mountain basin: Peter Sinks, Utah. *J. Appl. Meteor.,* **42,** 752–768.

Daly, C., W. Gibson, G. Taylor, G. Johnson, and P. Pasteris, 2002: A knowledge-based approach to the statistical mapping of climate. *Climate Res.,* **22,** 99–113.

Doran, J. C., and T. W. Horst, 1983: Observations and models of simple nocturnal slope flows. *J. Atmos. Sci.,* **40,** 708–717.

——, and S. Zhong, 1994: Regional drainage flows in the Pacific Northwest. *Mon. Wea. Rev.,* **122,** 1158–1167.

Gustavsson, T., M. Karlsson, J. Bogren, and S. Sindqvist, 1998: Development of temperature patterns during clear nights. *J. Appl. Meteor.,* **37,** 559–571.

Haiden, T., and C. D. Whiteman, 2005: Katabatic flow mechanisms on a low-angle slope. *J. Appl. Meteor.,* **44,** 113–126.

Heywood, G. S. P., 1933: Katabatic winds in a valley. *Quart. J. Roy. Meteor. Soc.,* **59,** 43–57.

Hocevar, A., and J. D. Martsolf, 1971: Temperature distribution under radiation frost conditions in a central Pennsylvania valley. *Agric. For. Meteor.,* **8,** 371–383.

Kimura, F., and T. Kuwagata, 1993: Thermally induced wind passing from plain to basin over a mountain range. *J. Appl. Meteor.,* **32,** 1538–1547.

Kurita, H., H. Ueda, and S. Mitsumoto, 1990: Combination of local wind systems under light gradient wind conditions and its contribution to the long-range transport of air pollutants. *J. Appl. Meteor.,* **29,** 331–348.

LeMone, M. A., K. I. Ikeda, R. L. Grossman, and M. W. Rotach, 2003: Horizontal variability of 2-m temperature at night during CASES-97. *J. Atmos. Sci.,* **60,** 2431–2449.

Lenschow, D. H., B. B. Stankov, and L. Mahrt, 1979: The rapid morning boundary-layer transition. *J. Atmos. Sci.,* **36,** 2108–2124.

Liston, G. E., R. A. Pielke Sr., and E. M. Greene, 1999: Improving first-order snow-related deficiencies in a regional climate model. *J. Geophys. Res.,* **104,** 19 559–19 567.

Magono, C., C. Nakamura, and Y. Yoshida, 1982: Nocturnal cooling of the Moshiri Basin, Hokkaido in midwinter. *J. Meteor. Soc. Japan,* **60,** 1106–1116.

Mahrt, L., and R. Heald, 1983: Nocturnal surface temperature distribution as remotely sensed from low-flying aircraft. *Agric. For. Meteor.,* **28,** 99–107.

——, and D. Vickers, 2005: Boundary-layer adjustment over small-scale changes of surface heat flux. *Bound.-Layer Meteor.,* **116,** 313–330.

——, ——, R. Nakamura, J. Sun, S. Burns, D. Lenschow, and M. Soler, 2001: Shallow drainage and gully flows. *Bound.-Layer Meteor.,* **101,** 243–260.

Moore, I. D., T. W. Norton, and J. E. Williams, 1993: Modelling environmental heterogeneity in forested landscapes. *J. Hydrol.,* **150,** 717–747.

Nakamura, R., and L. Mahrt, 2005: Air temperature measurement errors in naturally ventilated radiation shields. *J. Atmos. Oceanic Technol.,* **22,** 1046–1058.

Nie, D., T. Demetriades-Shah, and E. T. Kanemasu, 1992: Surface energy fluxes on four slope sites during FIFE 1988. *J. Geophys. Res.,* **97,** 18 641–18 649.

Pielke, R. A., and P. Mehring, 1977: Use of mesoscale climatology in mountainous terrain to improve the spatial representation of mean monthly temperatures. *Mon. Wea. Rev.,* **105,** 108–112.

Richardson, A. D., X. Lee, and A. J. Friedland, 2004: Microclimatology of treeline spruce-fir forests in mountains of the northeastern United States. *Agric. For. Meteor.,* **125,** 53–66.

Schwarz, P. A., B. E. Law, M. Williams, J. Irvine, M. Kurpius, and D. Moore, 2004: Climatic versus biotic constraints on carbon and water fluxes in seasonally drought-affected ponderosa

pine ecosystems. *Global Biogeochem. Cycles,* **18,** GB4007, doi:10.1029/2004GB002234.

Stewart, J. Q., C. D. Whiteman, W. J. Steenburgh, and X. Bian, 2002: A climatological study of thermally driven wind systems of the U.S. intermountain West. *Bull. Amer. Meteor. Soc.,* **83,** 699–708.

Tabony, R. C., 1985: Relations between minimum temperature and topography in Great Britain. *J. Climatol.,* **5,** 503–520.

Thorton, P., S. Running, and M. White, 1997: Generating surfaces of daily meteorological variables over large regions of complex terrain. *J. Hydrol.,* **190,** 214–251.

Vickers, D., and L. Mahrt, 1997: Quality control and flux sampling problems for tower and aircraft data. *J. Atmos. Oceanic Technol.,* **14,** 512–526.

——, and ——, 2006: A solution for flux contamination by mesoscale motions with very weak turbulence. *Bound.-Layer Meteor.,* **118,** 431–447.

Whiteman, C. D., 2000: *Mountain Meteorology.* Oxford University Press, 355 pp.

——, and T. B. McKee, 1982: Breakup of temperature inversions in deep mountain valleys. Part II: Thermodynamic model. *J. Appl. Meteor.,* **21,** 290–302.

——, K. J. Allwine, L. J. Fritschen, M. M. Orgill, and J. R. Simpson, 1989: Deep valley radiation and surface energy budget microclimates. Part II: Energy budget. *J. Appl. Meteor.,* **28,** 427–437.

——, X. Bian, and S. Zhong, 1999: Wintertime evolution of the temperature inversion in the Colorado plateau basin. *J. Appl. Meteor.,* **38,** 1103–1117.

——, J. Hubbe, and W. Shaw, 2000a: Evaluation of an inexpensive temperature data logger for meteorological applications. *J. Atmos. Oceanic Technol.,* **17,** 77–81.

——, S. Zhong, X. Bian, J. D. Fast, and J. C. Doran, 2000b: Boundary layer evolution and regional-scale diurnal circulations over the Mexico basin and Mexican plateau. *J. Geophys. Res.,* **105,** 10 081–10 102.

Yoshino, M. M., 1975: *Climate in a Small Area.* Tokyo Press, 549 pp.

——, 1984: Thermal belt and cold air drainage on the mountain slope and cold air lake in the basin at quiet clear night. *Geo. J.,* **8,** 235–250.